Spontaneous Amyloidosis in LLC Mice

Renal Effects

C. K. Chai, PhD

Practically all low leukocyte count (LLC) mice over 1 year of age develop renal amyloidosis. Renal amyloid is deposited in the glomeruli and in the interstitium between the convoluted as well as collecting tubules, with consequent development of cysts and necrosis. LLC mice die of chronic renal failure. Electron microscopic studies reveal amyloid fibrils in the mesangium, a thickening of the basement membranes, and fusion of the foot processes in the glomeruli. Massive amounts of amyloid fibrils are also present in the interstitium, where intracellular fibrils in the fibroblasts as well as in the tubular epithelium cells are found. Vesicles, which are probably formed from membrane disruption, and amorphous materials are seen along the basement membranes. LLC mouse amyloidosis is discussed with regard to its potential as a model for studies on amyloidosis as well as the etiology and origin of amyloid fibrils. (Am J Pathol 90:381–398, 1978)

AFTER THE AGE OF 1 YEAR, all LLC (low leukocyte count) mice develop amyloidosis spontaneously. Amyloid deposits can be found in several organs: heavy deposition in the spleen, liver, adrenal gland, and kidney and lighter deposition in a number of other organs. A general description of this disease in LLC mice was given previously.[1] Because amyloidosis severely affects the kidneys of LLC mice, they eventually die of chronic renal failure. In this paper, a full description of the different stages of renal development will be presented. Renal lesions in LLC mice resemble those in some humans.[2] The LLC mouse is more severely affected than any other animal reported.

Materials and Methods

The mice used in this study are of the LLC line and are 9 or more months of age. In previous papers, both a brief and detailed history of their breeding [1,3] and a description of their biologic and genetic characteristics [4] have been reported. A maximum of 4 mice per pen are kept in a room at 21 ± 0.5 C (70 ± 1 F) and are given food (Purina Mouse Chow) and water *ad libitum*.

Light Microscopy

Mice are killed with CO_2, and an autopsy is immediately performed. Histologic preparations are made according to standard procedures: sectioning at 5 μ and staining with

From The Jackson Laboratory, Bar Harbor, Maine.

Supported by Grant CA 14036 from the National Cancer Institute and by an allocation from the research funds of the Jackson Laboratory.

The Jackson Laboratory is fully accredited by the American Association for Accreditation of Laboratory Animal Care.

Accepted for publication October 10, 1977.

Address reprint requests to Dr. Chen K. Chai, Senior Staff Scientist, The Jackson Laboratory, Bar Harbor, ME 04609.

hematoxylin and eosin. In questionable cases, crystal violet and Congo red staining procedures are employed to confirm the presence of the amyloid deposit.

Electron Microscopy

Small pieces of tissue are fixed in 0.1 M sodium cacodylate, pH 7.4, containing 2% glutaraldehyde and 1% paraformaldehyde, for 3 hours at room temperature. The tissues are washed in the same buffer overnight at 4 C and are then postfixed in that buffer with 1% OsO_4 for 2 hours at 4 C. Then the tissues are washed in two changes of a veronal acetate buffer, for 5 minutes each, followed by staining with 0.5% uranyl acetate in the veronal acetate buffer for 1 hour. After dehydration with ethanol and propylene oxide, the tissues are embedded in Epon. Sections are examined with a Hitachi HU-11C electron microscope operated at 75 kV.

Results

Eighty-seven mice were studied histologically for amyloid deposition and other pathologic changes in the kidney. The incidence of amyloidosis is recorded in Table 1; mice are grouped by age and are further classified according to the extent of amyloid deposition and other pathologic changes. The disease begins between 9 and 12 months of age. Ninety-five percent of the 1-year-old LLC mice had amyloid deposition in their kidney; this condition advances with age.

Gross Appearance

During the earlier stages of amyloidosis, the kidney may show slight indentations on the surface, which result from lesions developing in the cortex. As the disease advances, the kidney contracts, displaying a scarred or granular subcapsular surface (Figure 1). Nodules of various sizes resulting from cyst formation protrude from the kidney surface; fluid accumulates under the capsules. Both kidneys are similarly affected.

Light Microscopy

Different degrees of amyloid deposition in LLC mice are illustrated in Figure 2. The plates are arranged in a sequence which represents the

Table 1—Number of LLC Mice With Different Degrees of Amyloid Deposition and Other Lesions in the Kidney, as Found in Different Age Groups

Age (months)	No. of mice	Degrees of amyloid deposition and other lesions*			
		−	+	++	+++
9–12	13	9	4	0	0
12–18	53	3	24	12	14
≥18	21	0	4	6	11

−−, no amyloid was found; +, traces if amyloid and small numbers of cysts were present; ++, amyloid, cysts, and necrosis appeared in approximately one third of a section; +++, the above pathologic changes covered approximately one half or more of a kidney section.

gradual advancement of this disease. The proliferation of interstitial cells and the loss of glomeruli and tubules in the cortex are depicted in Figure 2A. We assume that the traces of amyloid deposits (not visible in the figure) found in the interstitium and glomeruli represent the beginnings of amyloidosis development. As the condition advances, amyloid deposits form a radial pattern in the outer zone of the medulla (Figure 2B); this pattern is characteristic of amyloid development in LLC mice. The pattern, at first more noticeable between collecting tubules, later extends into some areas of the cortex (Figure 2C). Parallel with the extension of amyloid deposition in the cortex is the formation of cysts. Cysts develop from glomeruli as a result of the expansion of the Bowman's capsule, accompanied by simultaneous atrophy and loss of glomeruli. With further progression of this disease, amyloid deposits and cysts appear throughout the entire kidney, rendering the radial patterns indistinguishable (Figures 2D and 2E). However, we noticed that some tubules still remain intact. As the disease approaches its terminal stages (Figure 2E), cysts and scars replace most of the kidney's normal tissues (Figure 2F).

In the glomeruli, amyloid deposition originates in the mesangial region, concomitant with the formation of cysts. Heavy deposition, however, is seen only occasionally (Figure 3A). Glomerular atrophy, amyloid deposition, and cyst formation are presumed to develop simultaneously; thus, most glomeruli disappear before large amounts of amyloid are deposited. In the interstitium, however, amyloid accumulates continuously, replacing normal tissues, and this results in large areas of amyloid interspersed among fibroblasts. A typical example of such an area, appearing crystal-like with the light microscope, is illustrated in Figure 3B. Amyloid deposition also occurs in the papilla of the kidney of LLC mice; in severe conditions it replaces the collecting tubules (Figure 3C) and forms an "amyloid skeleton."

In the amyloidotic kidneys, lesions with fibrosis, thickened capillaries, and glomerular sclerosis (Figure 3D) are frequently seen; these contain few or no amyloid deposits.

Electron Microscopy

Amyloid fibrils are found in the mesangium of the glomeruli of the LLC mouse kidneys (Figures 4A and 4B). The mesangium tends to be swollen, and fusion of the foot processes of the potocytes can be seen. Although subendothelial or subepithelial amyloid fibrils have not been discovered, amyloid fibrils attached to the thickened basal lamina of the Bowman's capsule are frequently observed in close association with pericapsular, interstitial amyloid deposits (inset in Figure 4B).

Confirming the light microscopic findings, massive depositions of amyloid fibrils are seen in the interstitial space of the tubular regions (Figure 5A). The capillaries are surrounded and compressed by amyloid fibrils; some parts of their basement membranes become indistinguishable (Figure 5A). The presence of fibrils in the cytoplasm of fibroblasts is seen frequently (Figure 5B). Thickened basement membranes and disrupted cytoplasmic membranes of the tubular epithelial cells often occur in regions where amyloid is present in the interstitium. We found amyloid fibrils among the disrupted membranes, interspersed with membrane vesicles which probably resulted from membrane disruption (Figure 5C). We also noticed the presence of amorphous material along the basement membrane, infiltrating between the mitochondria as well as along the cytoplasmic infoldings (Figure 5D).

Discussion

The development of amyloidosis in LLC mice involves a large number of organs, with heavy amyloid deposition in the spleen, liver, adrenal gland, and kidney and less deposition in various other organs. Among all these organs, I believe that amyloid deposition in the kidney is the primary factor contributing to the death of these mice.

On the basis of amyloid tissue localization, Zschiesche [5] attempted to classify spontaneous murine amyloidosis into two types: Type I, associated with malignant or inflammatory lesions, is characterized by subintimal amyloid deposition in the walls of small blood vessels, perifollicular distribution in the spleen, and glomerular localization in the kidney. Type II displays predominant interstitial renal, sinusoidal liver, and red pulp splenic amyloid, without displaying underlying diseases. In LLC mice, the predominant amyloid deposition in the renal interstitium and liver sinusoids, as well as mass deposition throughout the spleen, adrenal cortex, and several other organs,[4] seems to correspond most closely to the characteristics Zschiesche outlined for Type II. However, amyloid is present in the adventitia of blood vessels in the lung, heart, and pancreas. Scheinber et al [6] similarly found it difficult to easily classify the SJL/J amyloidosis which they observed in either type, because SJL/J mice with lymphoproliferative neoplasms also developed interstitial renal and sinusoidal liver amyloid deposits. If a genetic basis does underlie each type, Zschiesche [5] should not have found two different types within the same, well-established inbred strain. Further studies of the histopathologic changes in conjunction with a genetic analysis of spontaneous amyloidosis will be needed for clarification.

My present findings on the distribution of amyloid fibrils in the kidney

of LLC mice closely resemble those reported cases in humans.[2,7] Although LLC mice have more amyloid deposits in the tubular region and less in the glomeruli than do humans, the major sites of deposition (such as the mesangium and the interstitium) are the same in animals and humans. I have found neither subendothelial nor subepithelial amyloid fibrils nor fibrils in the lumen of the glomerular capillaries, but the massive amount of amyloid fibrils seen in the interstitium of the LLC mice is striking.

The simultaneous development of glomerular cysts is assumed to be a result of renal amyloidosis. Functional impairment in water resorption results from amyloid deposition in the interstitial spaces of the tubules. The back pressure of the water content of the tubules, in addition to the poor circulation resulting from amyloid deposition around the capillaries, will synergetically speed up cyst formation and glomerular atrophy. The destruction of glomeruli and tubular epithelium is, of course, fatal.

The nature of the amorphous material in the tubule region (and in the mesangium in small amounts) remains to be determined. This material may consist of immunoglobulin-like substances. The hypothesis is based on evidence of an overall increase in the level of different classes of immunoglobulins in old LLC mice [4] and a positive reaction with immunofluoresceins labeled "polyvalent immunoglobulin antibodies" in both the glomeruli and tubule regions.[4] The high level of immunoglobulins may be interpreted as a consequence of autoimmunity of a separate disease occurring simultaneously with amyloidosis. On the other hand, the possibility that immunoglobulin-like materials are chemical components of the amyloid fibrils in LLC mice should not be excluded. These speculations are under investigation.

Reviewing the developmental history and biologic characteristics of LLC mice, I believe that the low leukocyte level is the basis of their various immunologic problems. One such problem has been dealt with here: the development of amyloidosis at a high rate in early age with involvement of several organs and with the most severe effects in the kidney. These characteristics of amyloidosis, not previously reported in any other animal, make the LLC mouse an animal model well suited for amyloidosis research.

References

1. Chai CK: Reticular cell hyperplasia and amyloidosis in a line of mice with low leukocyte counts. Am J Pathol 85:49–72, 1976
2. Wellington J, Pirani CL: Renal amyloidosis: Electron microscopic observations. Acta Path Microbiol 80(suppl 233):217–227, 1972
3. Chai CK: Selection for leukocyte counts in mice. Genet Res 8:125–142, 1966
4. Chai CK: Biological and pathological characteristics in mouse lines with large

differences in leukocyte counts. The Reticuloendothelial System in Health and Disease. Edited by H Friedman, MR Escobar, SM Reichard. New York, Plenum Publishing Corp., 1976, pp 279–288
5. Zschiesche W: Spontaneous amyloidosis of the mouse. 3. Two patterns of amyloid distribution and their pathogenic relationship. Acta Pathol Microbiol Scand [A] 233:135–140, 1972
6. Scheinber MA, Cathcart ES, Eastcott JW, Skinner M, Benson M, Shirahama T, Bennett M: The SJL/J mouse: A new model for spontaneous age-associated amyloidosis. Lab Invest 35:47–54, 1976
7. Shirahama T, Cohen AS: Fine structure of the glomerulus in human and experimental renal amyloidosis. Am J Pathol 51:869–911, 1967

Acknowledgments

The author wishes to thank Thomas Farley for managing the mouse colony and conducting the autopsies and Lester Bunker and his associates for histologic service. The author is particularly grateful to Dr. J. J. Eppig and H. Reuther for the electron microscopic work and to Dr. D. R. Coman for consultation.

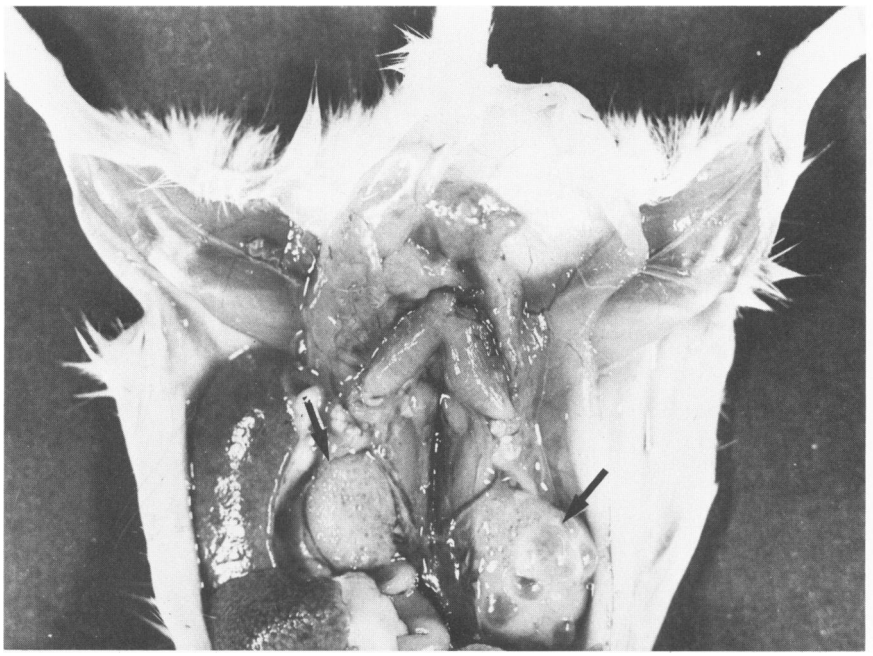

1

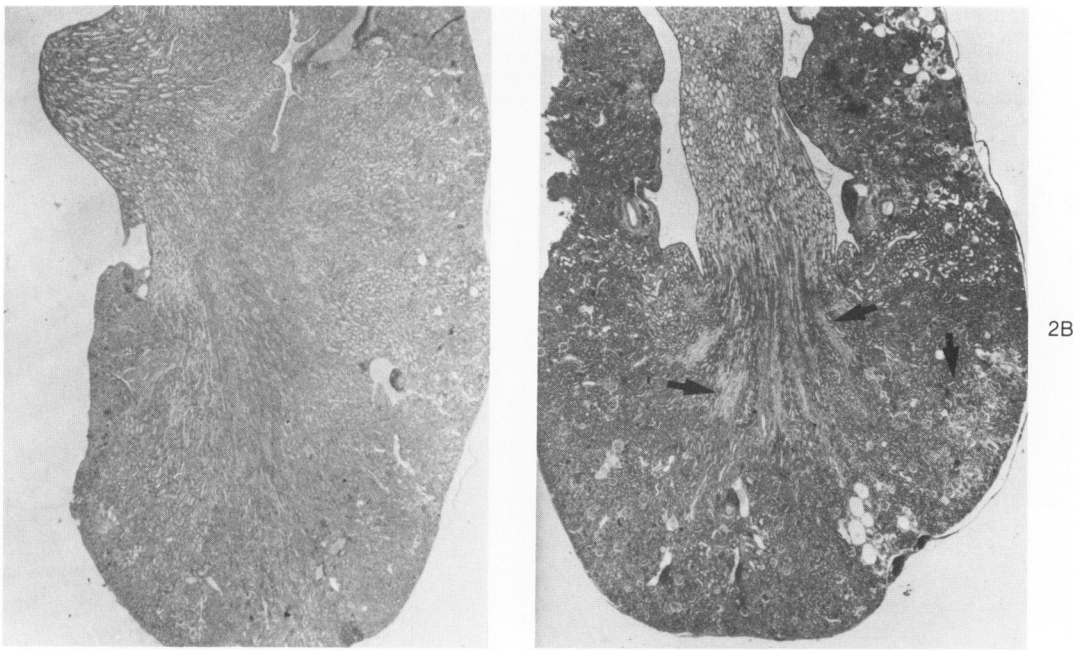

2A 2B

Figure 1—Gross appearance of kidneys (*arrows*) of an amyloidotic 14-month-old LLC female mouse. Note the large cysts in the kidney on the left and the granularities and contractions in both of them. **Figure 2**—Kidney sections of LLC mice at low magnification, showing different stages of amyloidosis and associated pathologic changes. (× 30). **A**—Tubular epithelial necrosis and fibrosis begin to appear in regions of the cortex which show indentations. Only traces of amyloid deposits can be seen between the tubules and occasionally in the glomeruli (not visible in the figure). **B**—Glomerular cysts and noticeable amounts of amyloid deposits (*arrows*) in the cortex and medulla. Conditions of **A** and **B** were recorded as +.

Figure 2C—A greater number of larger cysts and greater amounts of amyloid deposits than in **B**. Note the radial pattern of amyloid deposition. Leukocyte infiltration is present (*upper right*). The condition was recorded as + +. **D**—Massive amyloid deposition, cyst formation, fibrosis, and, consequently, little normal tissue. **E**—Amyloid in the cystic and necrotic regions is not as abundant as in **D**. Less than 50% of the normal tissue remains, approaching the terminal stage. **F**—Large cysts, kidney atrophy, and deformation; most of the normal tissue is destroyed. Amyloid deposits are still seen in some areas. Conditions shown in **D, E,** and **F** are recorded as + + +.

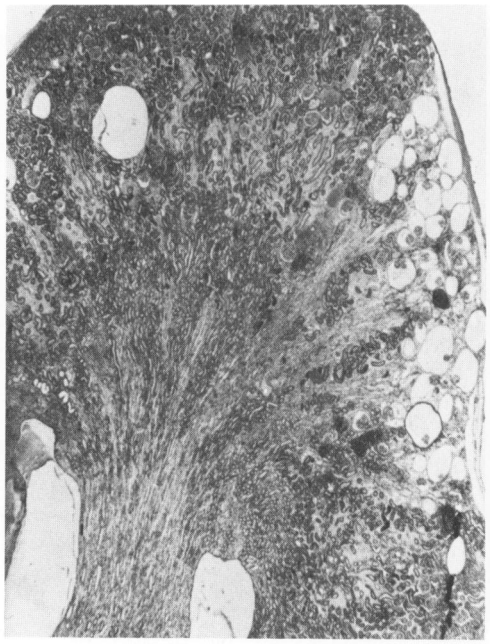

2C

2D

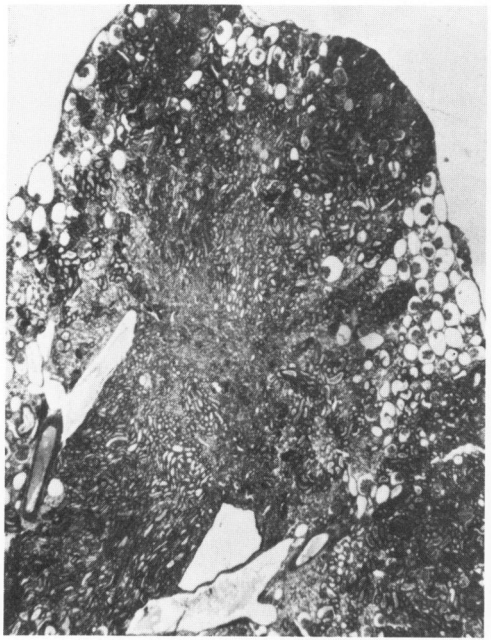

2E

2F

3A

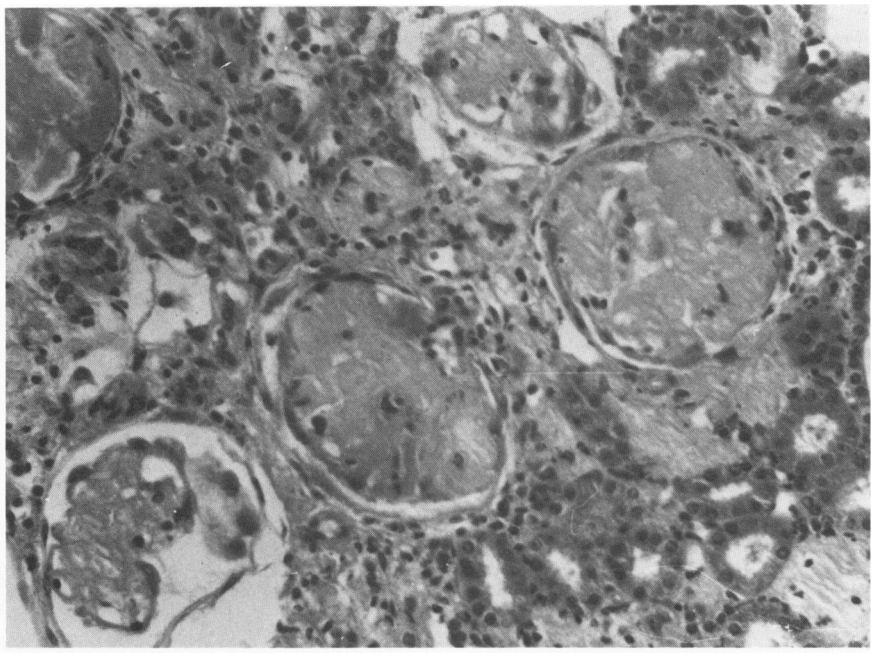

3B

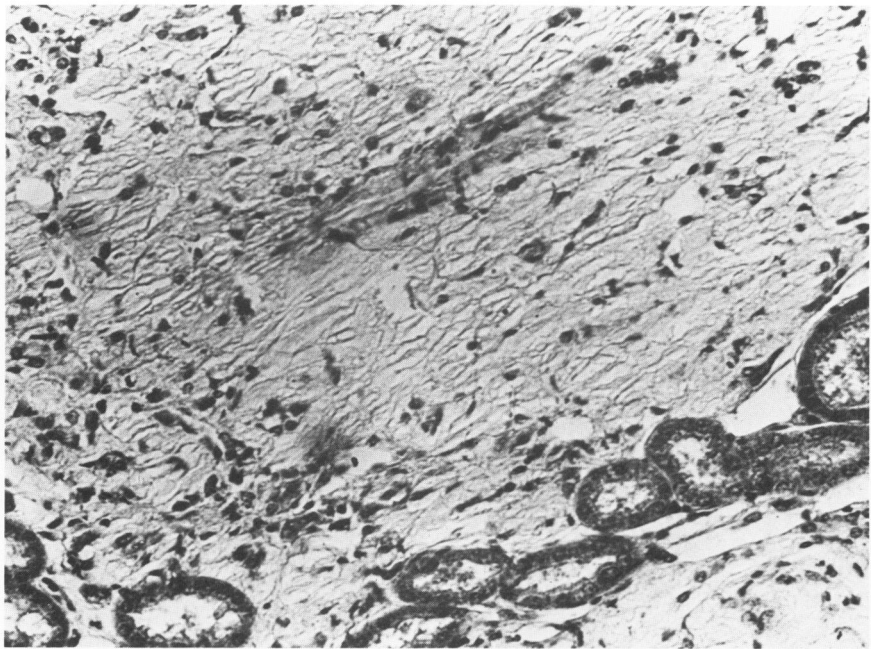

Figure 3—Higher magnification than in Figure 2, showing details of pathologic changes. **A**—Amyloid deposition replaces most of the capillaries in the glomeruli. **B**—Characteristic crystal appearance of amyloid deposits interspersed with fibroblasts most frequently seen in the upper zone of the medulla. Remaining tubular epithelium appears to be intact.

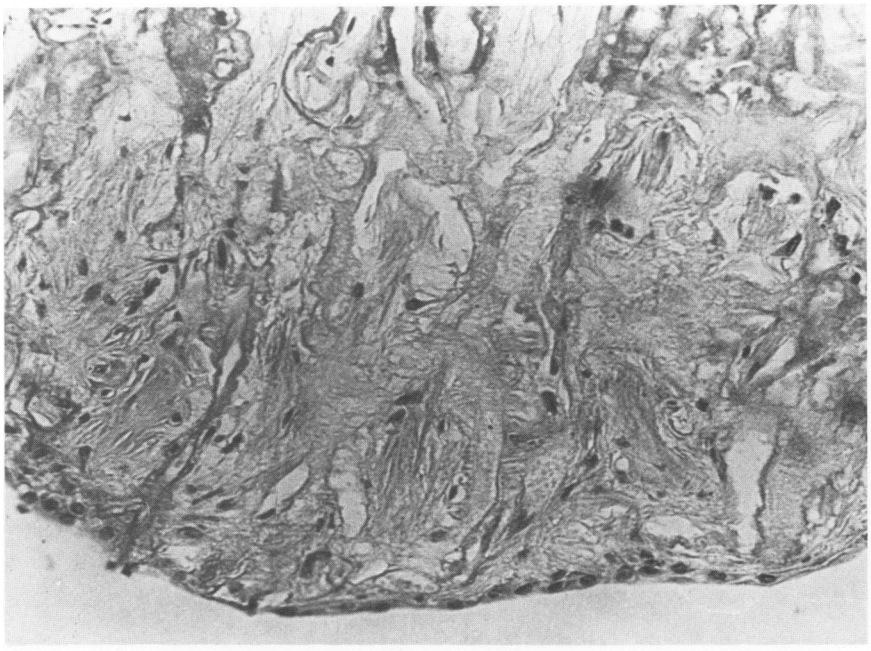

3C

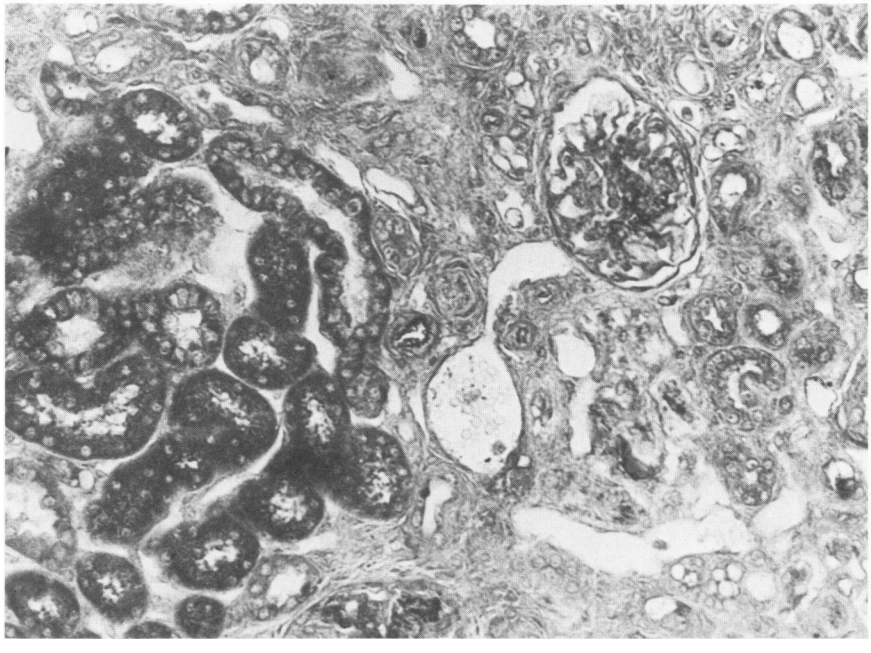

3D

Figure 3C—Amyloid deposition replaces most of the tubule structures in the papilla. **D**—Fibrosis, glomerular sclerosis, and thickening of arteriolar and capillary walls.

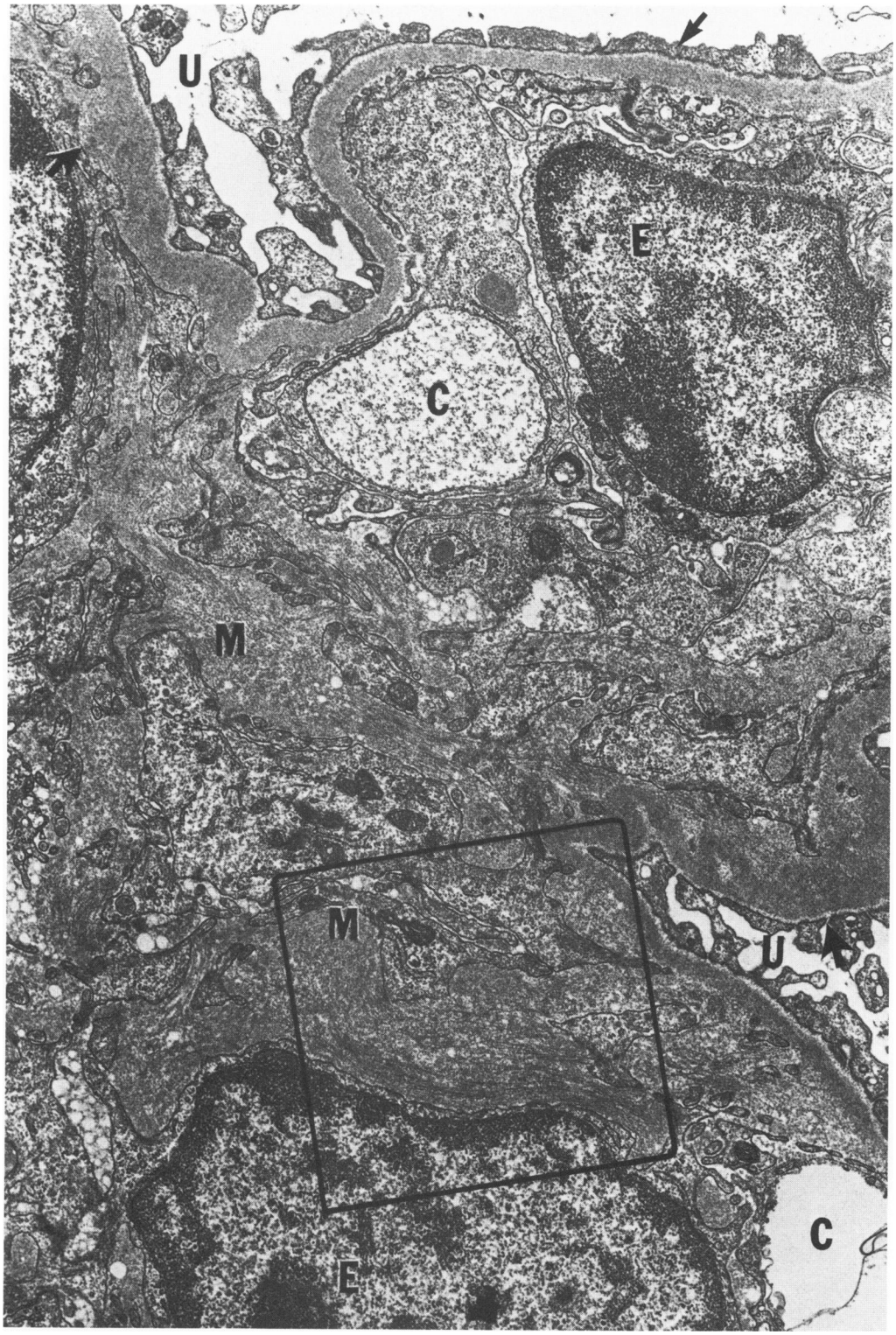

Figure 4A—Mesangial region of an LLC mouse glomerulus. Amyloid fibrils in the mesangium (*M*). Thickening of the basement membrane (*large arrow*) and fusion of the foot processes of a potocyte (*small arrow*). *U* = urinary space; *C* = capillary lumen; *E* = endothelial cell. Enclosed area is magnified in **4B**. (× 14,000)

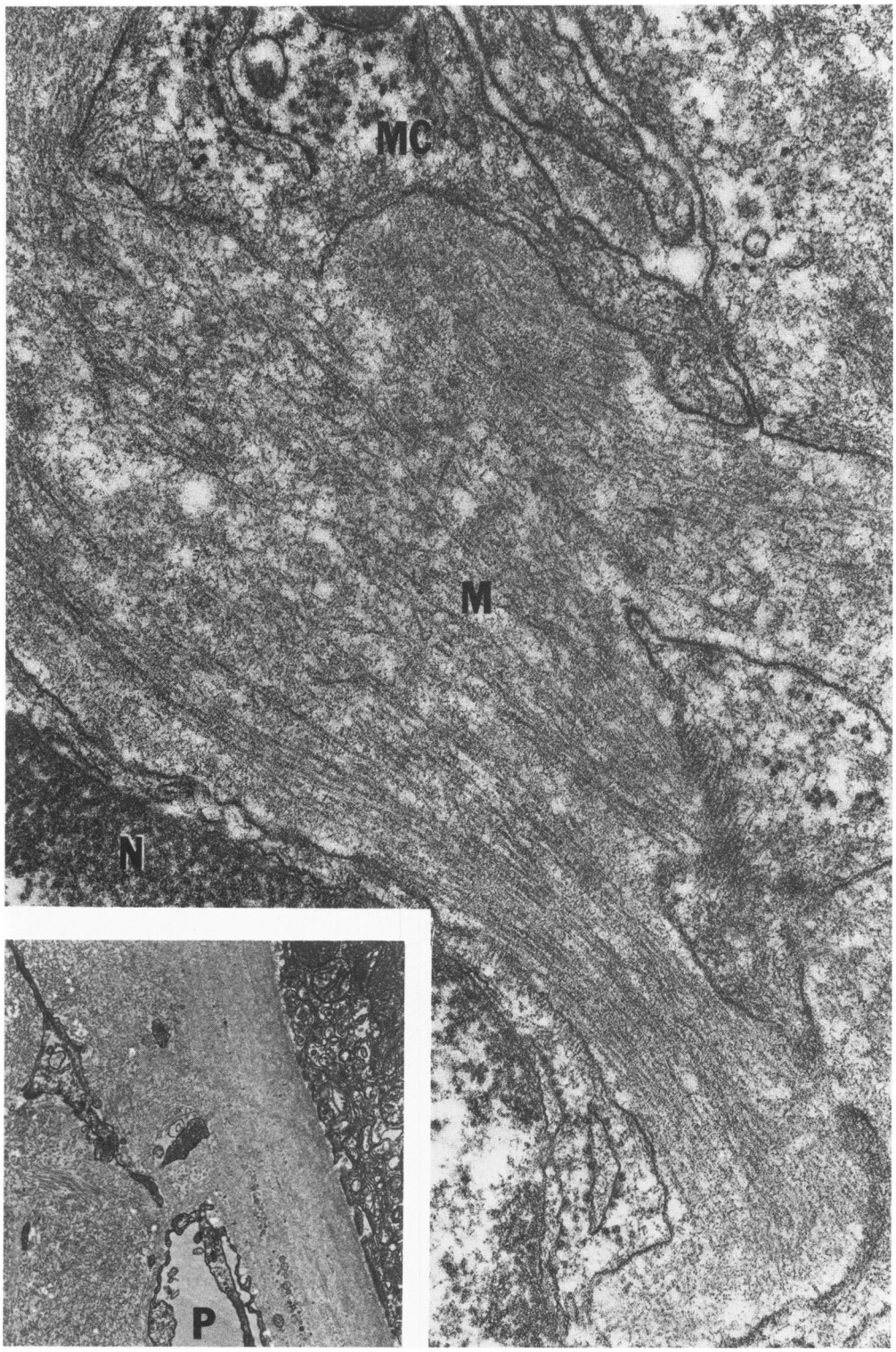

Figure 4B—Mesangial region of a field from **4A**, showing amyloid fibrils in the mesangium. *N* = endothelial cell nucleus; *M* = mesangium; *MC* = mesangial cell process. (× 64,000) **Inset**—Thickening of Bowman's capsule and amyloid fibrils attached to the parietal side (*P*).

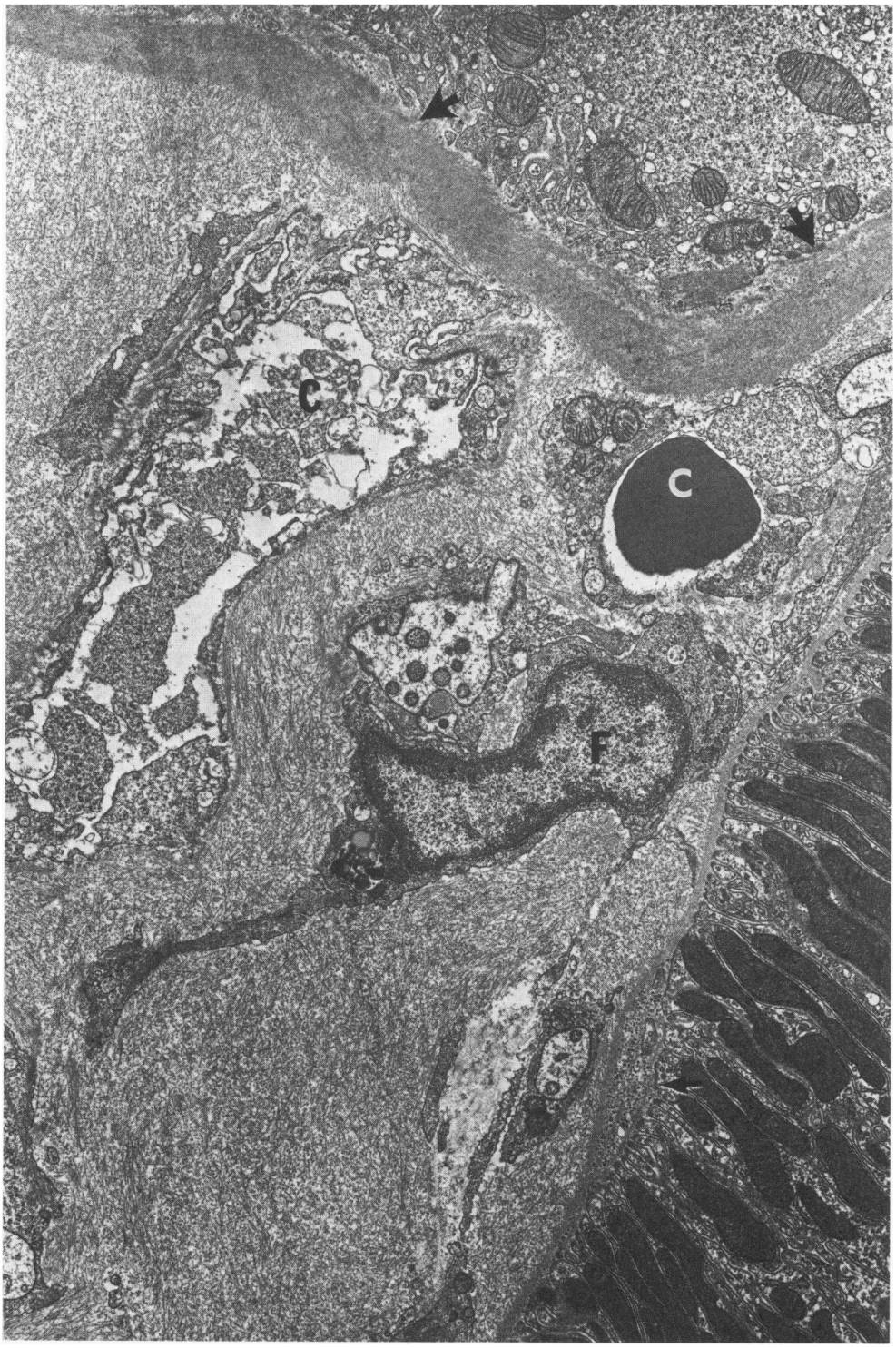

Figure 5A—Amyloid fibrils in the interstitial space of the tubular region of an LLC mouse kidney. At the top, slight thickening of the basement membrane (*large arrow*) of a proximal tubule. The cytoplasm in the *lower right corner* is that of a cell of the thick ascending limb of Henle's loop. Note lifting and disruption of the cytoplasmic membrane (*small arrow*). The capillaries are surrounded by a mass of amyloid fibrils. *C* = capillary; *F* = fibroblast. (× 9700)

Figure 5B—Amyloid fibrils in the interstitium and an interstitial cell cytoplasmic process with distended rough endoplasmic reticulum and densely packed fibrils. Note fibrils in the loosely packed area (*arrow*) with a morphologic resemblance to the extracellular fibrils. In many fuzzy regions of the cytoplasmic membrane, fibrils appear to cross between intracellular and extracellular space. (× 66,000)

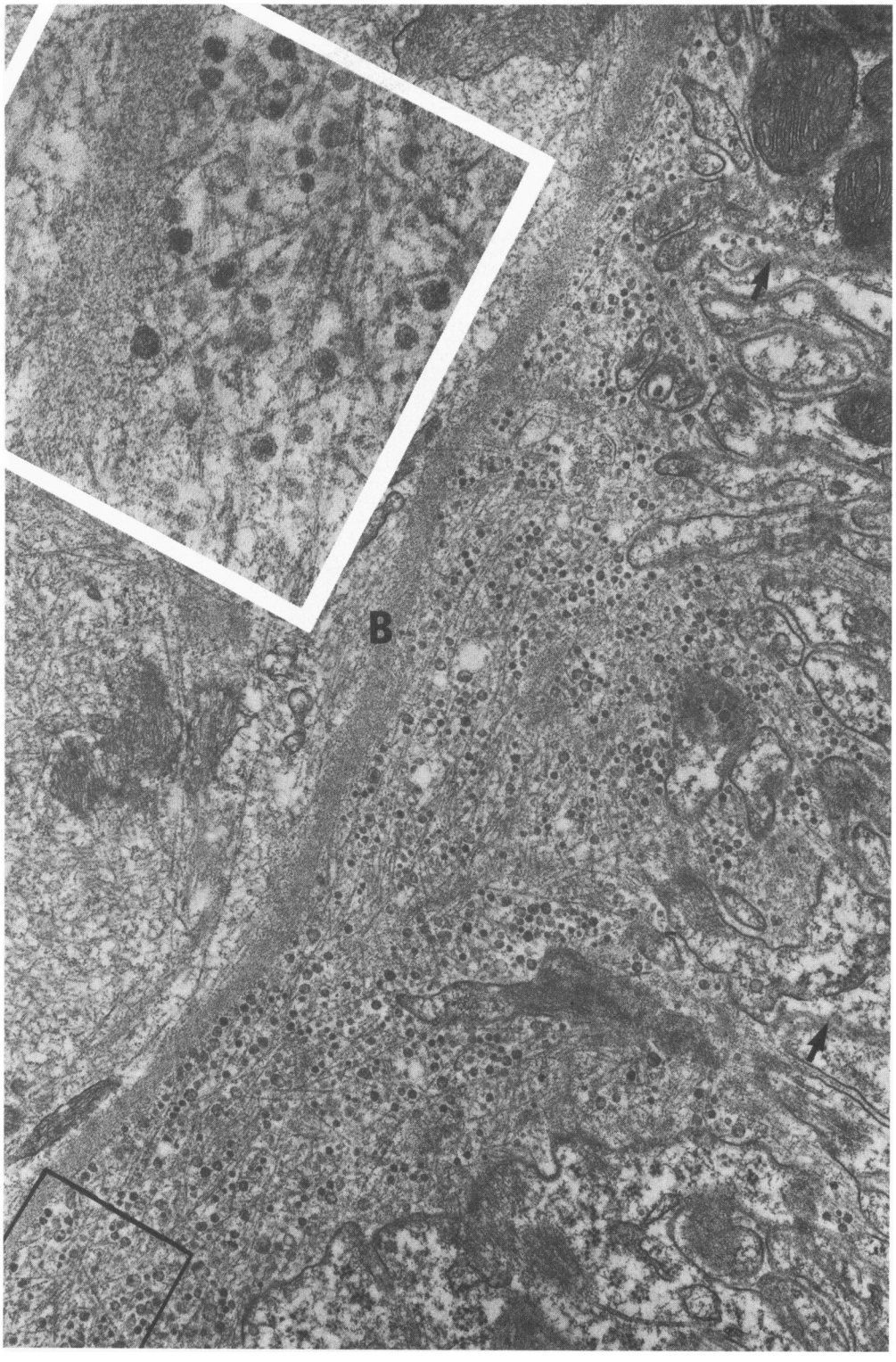

Figure 5C—Amyloid fibrils in both sides of the basement membrane (*B*) of Henle's ascending limb. Vesicles (probably formed from plasma membrane disruption) interspersed in the amyloid fibrils. Some amorphous materials penetrate between the mitochondria and into the infoldings (*arrow*). **Inset**—Higher magnification, illustrating a portion of the disrupted membrane revealing in more detail the morphology of the vesicles and amyloid fibrils. Note the apparent double-stranded structures of the fibrils. (× 29,200)

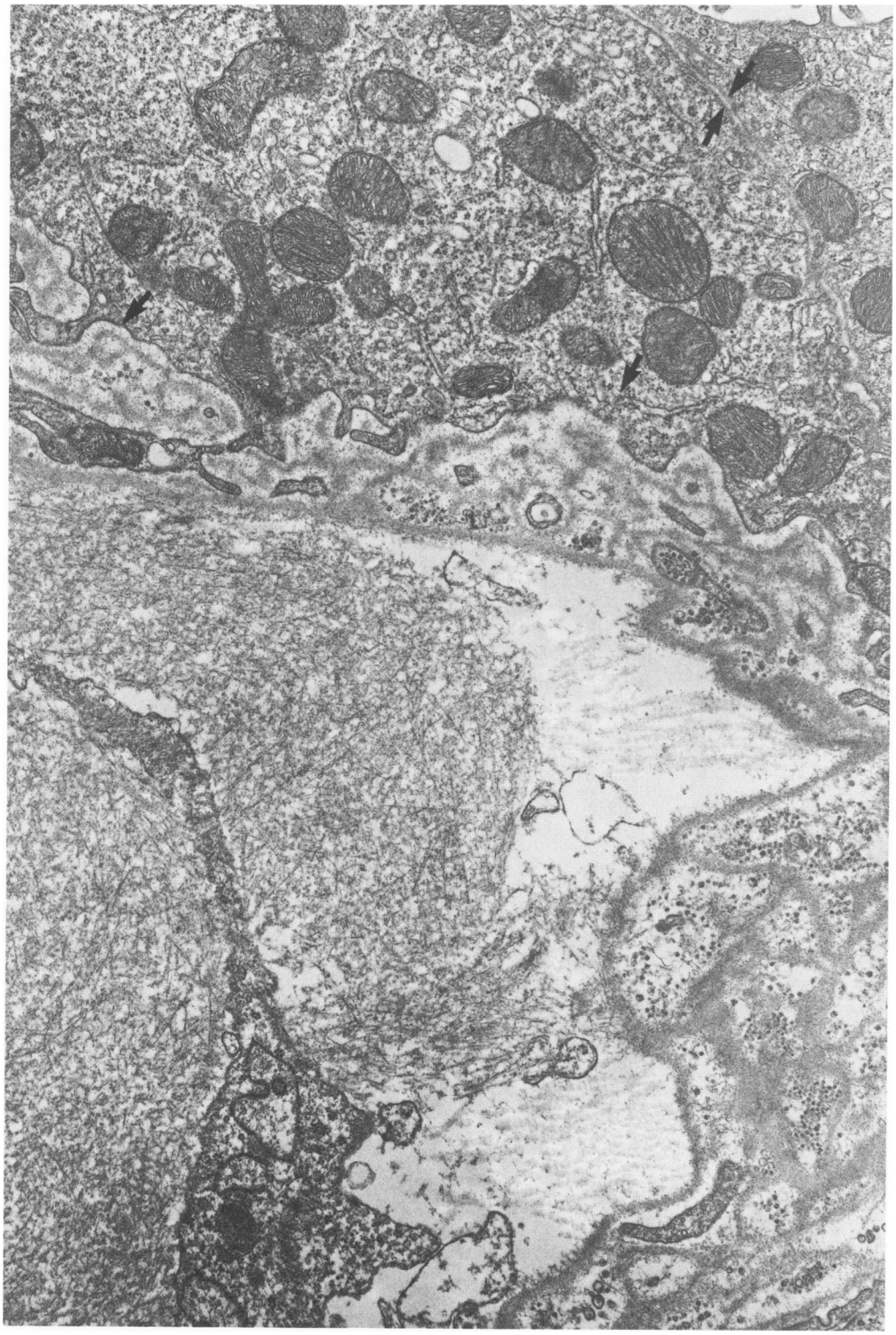

Figure 5D—Electron-dense amorphous material along the basement membrane of a proximal tubule cell and amyloid fibrils in the interstitial space. Vesicles formed from the plasma membrane disruption enclosed by the amorphous material (*arrow*). Epithelium cell interdigitation (*facing arrows*). (× 19,400)

[*End of Article*]